

Systematic Approach to DNA Aptamer Design Using Amino Acid–Nucleic Acid Hybrids (ANHs) Targeting Thrombin

Ji Hye Yum^{1,‡}, Takumi Ishizuka^{3,‡}, Koyuki Fukumoto¹, Daisuke Hori¹, Hong-Liang Bao³, Yan Xu³, Hiroshi Sugiyama^{1,2,}, and Soyoung Park^{1,*}*

¹Department of Chemistry, Graduate School of Science, Kyoto University,
Kitashirakawa-oiwakecho, Sakyo-ku, Kyoto 606-8502, Japan

²Institute for Integrated Cell-Material Sciences (iCeMS), Kyoto University, Yoshida-
ushinomiyacho, Sakyo-ku, Kyoto 606-8501, Japan

³Department of Medical Sciences, Faculty of Medicine, University of Miyazaki, 5200
Kihara, Kiyotake, Miyazaki 889-1692, Japan

**Corresponding author:* Dr. Soyoung Park, Prof. Dr. Hiroshi Sugiyama

Tel.: (+)81-75-753-4002; Fax: (+)81-75-753-3670

E-mail: oleesy@kuchem.kyoto-u.ac.jp, hs@kuchem.kyoto-u.ac.jp (H.S.)

Received Date: (to be automatically inserted after your manuscript is accepted if required according to the journal that you are submitting your paper to)

KEYWORDS

DNA aptamer, Chemical modification, Amino acid residues, Thrombin binding aptamer

Abstract

Chemical modifications of innate DNA/RNA aptamers facilitate the improvement of their function. Herein, we report our modular strategy to manipulate a thrombin-binding DNA aptamer (TBA) to improve its anticoagulation activity and binding affinity. A set of amino acid conjugates, termed amino acid–nucleic acid hybrids or ANHs, was synthesized and incorporated into TBA loop sequences. We found that substitutions with hydrophobic amino acids in the loop region possessed significantly enhanced antithrombin activity, up to threefold higher than the native TBA. We investigated the correlations between thrombin-binding affinity and the features of our amino-acid conjugates using experimental techniques including circular dichroism spectroscopy, surface plasmon resonance assay and molecular modeling. The present study demonstrates a systematic approach to aptamer design based on amino-acid characteristics, allowing the development of advanced aptamers.

Introduction

The rapid development of innovative biochemical tools has demonstrated that DNA and RNA are more than simple genetic materials and serve diverse and active roles that are relevant to interdisciplinary research (1). As a representative example, research into DNA and RNA aptamers has rapidly developed in parallel with the growth of SELEX technology (2). Because of their wide variety of target molecules, biocompatibility and susceptibility to chemical modification for functionalization (3), DNA and RNA aptamers have a broad range of prospective applications, including as biosensors, bioimaging, diagnostics, and therapeutics (4, 5). Numerous applications of aptamers have been reported. For instance, a hairpin ATP DNA aptamer showed excellent target specificity and, combined with nanomaterials, has been applied as a tool enabling switchable ATP release (6). In addition, structurally unique RNA aptamers that bind to HIV-1 reverse transcriptase and interfere with its biological functions have been investigated (7). In addition to the common hairpin structures, G-quadruplex (G4) aptamers have been developed and have received extensive attention because of their improved biocompatibility and higher cellular uptake efficiency (8). These benefits have led biochemists to investigate a wide range of G4-based aptamers for protein detection, activity regulation and therapeutic purposes (9). One example of a G4 aptamer under clinical trial is AS1411, a 26-nucleotide G4-forming DNA, which is in phase II trials for suppressing cancer cell proliferation by targeting nucleolin (10).

Thrombin binding aptamer (TBA) is the most well-known G4 DNA aptamer. It is folded from a short guanine-rich sequence (5'-d(GGTTGGTGTGGTTGG)-3') and exhibits a high degree of specificity and affinity for thrombin (11). Because of the importance of thrombin in the blood-clotting process and cell signaling pathways, TBA has undergone comprehensive investigation (12). Moreover, various types of functionalization of TBA, such as modifications of the sugar-phosphate backbone and bases, have been explored to improve the aptamer's properties, including its binding affinity, nuclease resistance and stability (Table S4). A set of modified sugars including (un)locked nucleic acids and a heteroatom-containing nucleotide (2'-F-araN) have been applied to TBA (13,14). The introduction of a sulfur atom to position 4 of uridine (4-thio-deoxyuridine, s4dU) and the substitution of an aromatic group into a guanine residue were demonstrated to increase binding affinity by reducing the polarity of TBA. The improved performance of these aptamers compared with the native sequence was demonstrated in an anticoagulation assay (15). In a recent study, Yang and coworkers reported the enhanced binding affinity of TBA incorporating a tryptophan-containing deoxyuridine (Trp-dU) into the loop region (16). Thus, site-specific chemical modification is a powerful tool for developing

advanced aptamers and expanding the range of the oligonucleotide pool. Moreover, Timofeev *et al.* have even extended the modified TBA library with carbohydrates. The installation of sugar rings on pyrimidine base in TBA15 displayed twofold higher affinity along with increased anticoagulation ability (17).

We have established a systematic modular strategy for chemical modification of oligonucleotides by incorporating metal-binding ligands into DNA oligonucleotides via an acyclic D-threoninol backbone. We introduced a bipyridine ligand into the DNA strands to generate DNA metalloenzymes and successfully demonstrated enantioselective hydration reactions (18). We have further advanced our modular approach using amino-acid residues and devised a family of unique biohybrid molecules that we termed amino acid–nucleic acid hybrids (ANHs) (19). Histidine-containing DNAs show superb metal-binding ability and excellent catalytic performance in DNA-based asymmetric catalysis as well as 2,2'-azino-bis(3-ethylbenzothiazoline-6-sulfonic acid) (ABTS) oxidation reactions. The incorporation of amino acid residues into DNA oligonucleotides endows new functions without disrupting the intrinsic features of nucleic acids. These results encouraged us to exploit ANH molecules as DNA aptamers.

In the present report, we outline our systematic design approach of using ANHs to generate DNA aptamers targeting thrombin. We chose a structurally and functionally well-defined TBA sequence (TBA15) as the basis for developing ANH-based TBA sets. The enhancement of anticoagulation activity associated with different modification sites and amino acid residues was clarified. Spectroscopic characterization, surface plasmon resonance (SPR) assays and molecular modeling studies provided information about the correlations between binding affinity and anticoagulation activity depending on the site-specific modification of amino acid residues.

Result and Discussion

<Figure 1>

The syntheses were performed using a condensation reaction between various commercially available Fmoc-protected L-amino acids (**1a–1g**) and a DMTr-protected acyclic D-threoninol (**2**), as shown in Figure 1B (see Supplementary Information (SI) for the details) (19, 20). In this study, we chose seven types of amino acids with different features and sizes: alanine (**1a**), phenylalanine (**1b**), histidine (**1c**), lysine (**1d**), methionine (**1e**), glutamine (**1f**) and tryptophan (**1g**) (21). The corresponding products (**3a–3g**) were obtained in moderate to good yields (45–86% yield).

Subsequent phosphitylation allowed the straightforward incorporation of amino acid residues into the DNA strands, 5'-d(GGTTGGTGTGGTTGG)-3'. The previously reported crystallographic study provides insight into the interaction between thrombin and the TBA loop (22). The thymines at positions 3, 4, 12 and 13 in the loop region play a principal role in thrombin (exosite I) binding. Therefore, systematic modification of these four thymine sites was performed using various ANH molecules. In total, 28 ANH-containing TBA variants, comprising seven different amino acid conjugates on each of the four thymine sites, were generated and identified by mass spectroscopy (Figure 1A, and see SI).

<Figure 2>

To obtain information about the conformation and the thermal stability of these ANH-based TBA sets, spectroscopic studies were performed (Figure 2 and SI). Circular dichroism (CD) spectra showed that all TBA variants formed antiparallel structures in the presence of potassium ions, indicated by a positive band near 290 nm and a negative band near 260 nm. Ellipticity and melting temperature varied depending on the amino acid residues and modification sites (16). These results support that the electric charge and the size of ANH building blocks affects to the DNA secondary structures' stability.

<Figure 3>

Structurally defined ANH-based TBAs have been exploited to evaluate thrombin inhibition (anticoagulation) activity using a prothrombin time (PT) assay, as illustrated in Figure 3A (23). For the experimental procedure, the native and modified TBA samples (final concentration 1 μ M) were preincubated in human plasma, then a thromboplastin reagent was supplied to the reaction solutions to initiate blood clotting. Here, prothrombin is activated to thrombin in the presence of the calcium ion. After triplicate assays, the average clotting time of each sample was calculated, and the results are listed in Figure 3B. In the absence of the DNA aptamer, fibrin formation is complete within 9.6 s. This time was doubled by the addition of the native sequence (as a positive control). We also conducted the PT assays using the ANH-based aptamers and observed interesting results depending on the modification sites and amino acid residues. Modification of thymines at positions 3 (T3) and 12 (T12) resulted in significant changes in clotting time that depended on the type of amino acid residue. Remarkably, TBA variants bearing hydrophobic amino acids (**Phe**, **Met** and **Trp**) exhibited dramatically improved anticoagulation activity when these replaced T3 or T12. The longest clotting time (60.2 s) was achieved with T3F TBA; this was sixfold higher than the negative control and threefold higher than the native sequence. **Met**- and **Trp**-ANH modifications elongated clotting time to 53.2 s and 45.5 s, respectively. By contrast,

the simplest aliphatic (**Ala**-), charged amino acids (**His**- and **Lys**-) or polar uncharged amino acid (**Glu**)-containing TBA variants produced less thrombin inhibition than the native TBA15. However, T4 and T13 substitutions with any type of amino acid residue resulted in no benefit for thrombin inhibition. It has been reported that T3 and T12 form hydrophobic interactions with amino acid residues of the fibrinogen binding site (exosite 1) of thrombin (24), while T4 and T13 form polar interactions. The enhanced anticoagulation activity of TBA variants bearing the hydrophobic amino acids (**Phe**, **Met** and **Trp**) at positions 3 and 12 of the loop region implies hydrophobic contact. In contrast, T4 and T13 modifications resulted in poorer performance than unmodified TBA15, despite the introduction of a hydrophilic amino acid (**Glu**).

<Figure 4>

We evaluated the nuclease resistance of ANH-modified TBAs using an endonuclease, DNase I. After the enzymatic reaction, a denaturation gel was used to confirm the cleavage. For single-stranded DNA, the full-length T3F DNA oligonucleotide partially remained, whereas the native DNA had completely digested (Figure 4A). In the presence of KCl, G-quadruplex formation efficiently protected both the native and ANH-modified aptamers from rapid nuclease digestion (Figure 4B). To investigate further, we performed SPR assays to quantify the binding affinity of DNA aptamers toward thrombin (Figure 5A). A set of 5'-biotinylated native or ANH-modified oligonucleotides were dissolved in HBS-EP buffer including 100 mM KCl for G-quadruplex formation. Three different sensor chips immobilized with each aptamer (RU = ~100) were prepared, and various concentrations of thrombin solutions (3.125–100 nM) passed over SA chips. The kinetic values including rates of association (k_a) and dissociation (k_d) were calculated from SPR sensorgrams according to 1:1 binding model-fitting methods. The parameters and affinity values are illustrated in Figure 5A. K_D was calculated to be 7.28 nM for the native TBA and 2.94 nM for T3F DNA, 2.5 times higher than the innate affinity. However, no significant binding was observed in the case of T4F DNA, as shown in Figure S9.

<Figure 5>

Consistent with the SPR results, the native gel image showed sequence-dependent protein binding (Figure 5B). an electrophoretic mobility-shift assay (EMSA) was carried out using FAM-labeled aptamer sets. As expected, protein–DNA complex bands appeared in the case of the native sequence and T3F. The T4F did not induce any specific band showing a binding interaction and only a G4 DNA band emerged. The DNA band for T4F was a smear even though we applied conditions identical to those used with other aptamers; this was attributed to the poor stability of T4F (Figure S7). We also generated molecular models of each aptamer to provide structural

information about the effect on thrombin binding of the amino-acid residue arrangement of ANH-modified aptamers. Energetically minimized models were prepared based on PDB files (ID: 1hao, 6EO6) (16, 22), and molecular dynamics was performed (see SI for details). ANH-based aptamers retained their overall structures, including the quadruplex core, but the configuration of each incorporated amino acid residue of the TBA variants relative to the amino acid of exosite 1 varied depending on the modified TBA (Figure 5C, for details see SI). Focusing on the T3 and T4 positions in the loop region, which mainly engaged in hydrophobic interactions with Tyr76, molecular modeling showed a hydrophobic interaction between the T3-substituted **Phe**-ANH aptamer and thrombin. In the case of T4F, the configurations and the binding modes were significantly altered from those of the unmodified TBA. The phenyl ring of the phenylalanine conjugate had completely flipped over from the G-quadruplex core and was excluded from the intermolecular interaction. These molecular modeling studies corroborate that the significant difference in anticoagulation activity between T3F and T4F is attributable to the binding affinity of ANH-modified TBA variants.

Conclusion

In conclusion, we generated a library of modified thrombin-binding aptamer sequences based on ANHs and investigated their anticoagulant activities. ANH-modified aptamers were designed systematically, and the straightforward synthetic approach facilitated the site-specific incorporation of amino acid building blocks into oligonucleotides through solid-phase DNA synthesis. All the TBAs generated formed antiparallel G-quadruplex structures regardless of the amino acid residue incorporated. ANH-aptamers including amino acids **Phe**, **Met** or **Trp** to replace the T3 of the loop region (T3F, T3M or T3W) demonstrated remarkably enhanced thrombin inhibition properties, which involved hydrophobic interactions between the amino acid of the modified TBA and the binding site of thrombin. Overall, we established the following series of processes: (1) selection of target aptamer sequences from databases; (2) rational design and site-specific functionalization with ANHs using our modular strategy; and (3) characterization and evaluation. We hope this ANH approach will serve as a promising alternative for resolving several obstacles to the use of present aptamers for clinical diagnostics and therapeutics. The development and evaluation of ANH-based DNA/RNA aptamers targeting various proteins and cells are ongoing in our laboratory.

ASSOCIATED CONTENT

Supporting Information

Synthetic routes of ANHs molecules threoninol conjugate, characterization data of new compounds, HPLC data, ESI-TOF-Mass data and CD spectra of oligonucleotides. This material is available free of charge via the Internet at <http://pubs.acs.org>.

Note

The authors declare no competing financial interest.

ACKNOWLEDGMENT

We express sincere thanks for a Grant-in-Aid Priority Research (16H06356 for H. S) from Japan Society for the Promotion of Science (JSPS). We also thank KAKENHI program (Grant-in-Aid for scientific research C, 18K05315) and Research Encouragement Grant from The Asahi Glass Foundation for support to S. P. We would like to thank Karin Nishimura (Graduate School of Engineering, Kyoto University) for technical assistance in obtaining the mass spectra of synthesized compounds. We wish to thank Dr. Atsushi Yamashita and Dr. Yujiro Asada

(Department of Pathology, Division of Pathophysiology, University of Miyazaki, Japan) for blood sampling and providing support to prothrombin time experiment.

REFERENCES

- (1) a) L. Gold, B. Polisky, O. Uhlenbeck, M. Yarus, *Annu. Rev. Biochem.* **1995**, *64*, 763–797.; b) N. C. Seeman, *Nature* **2003**, *421*, 427-431.
- (2) a) A. D. Ellington, J. W. Szostak, *Nature* **1990**, *346*, 818-822.; b) C. Tuerk, L. Gold, *Science* **1990**, *249*, 505-510.
- (3) a) C. L. Hamula, J. W. Guthrie, H. Zhang, X. F. Li, X. C. Le, *Trend. Anal. Chem.* **2006**, *25*, 681-691.; b) G. Mayer, *Angew. Chem. Int. Ed.* **2009**, *48*, 2672-2689.
- (4) a) B. Xu, C. Zhao, W. Wei, J. Ren, D. Miyoshi, N. Sugimoto, X. Qu, *Analyst* **2012**, *137*, 5483-5486.; b) J. Liu, Z. Cao, Y. Lu, *Chem. Rev.* **2009**, *109*, 1948-1998.; c) J. Mi, Y. Liu, Z. N. Rabbani, Z. Yang, J. H. Urban, B. A. Sullenger, B. M. Clary, *Nat. Chem. Biol.* **2010**, *6*, 22-24.; d) B. G. Nair, Y. Nagaoka, H. Morimoto, Y. Yoshida, T. Maekawa, D. S. Kumar, *Nanotech.* **2010**, *21*, 455102.
- (5) a) J. F. Lee, G. M. Stovall, A. D. Ellington, *Curr. Opin. Chem. Biol.* **2006**, *10*, 282-289.; b) Y. Zhu, P. Chandra, Y. B. Shim, *Anal. Chem.* **2013**, *85*, 1058-1064.; c) A. D. Keefe, A. Pai, A. Ellington, *Nat. Rev. Drug Discov.* **2010**, *9*, 537-550.; d) H. Jo, H. Gu, W. Jeon, H. Youn, J. Her, S. K. Kim, J. Lee, J. H. Shin, C. Ban, *Anal. Chem.* **2015**, *87*, 9869-9875.

- (6) a) D. S. Wilson, J. W. Szostak, *Annu. Rev. Biochem.* **1999**, *68*, 611-647.; b) J. Wang, Y. Jiang, C. Zhou, X. Fang, *Anal. Chem.* **2005**, *77*, 3542-3546.
- (7) X. Ye, A. Gorin, A. D. Ellington, D. J. Patel, *Nat. Struct. Biol.* **1996**, *3*, 1026-1033.
- (8) a) O. W. Tucker, T. K. Shum, A. J. Tanner, *Curr. Pharm. Design* **2012**, *18*, 2014-2026.; b) C. Roxo, W. Kotkowiak, A. Pasternak, *Molecules* **2019**, *24*, 3781.
- (9) a) S. Nagatoishi, D. Miyoshi, N. Sugimoto, *Int. Rev. Biophys. Chem.* **2011**, *2*, 129-134.; b) B. Fu, Y. Park, K. T. Kim, K. Chen, G. Zou, Q. Wei, ... X. Zhou, *Chem. Commun.* **2018**, *54*, 11487-11490.
- (10) a) J. E. Rosenberg, R. M. Bambury, E. M. Van Allen, H. A. Drabkin, P. N. Lara, A. L. Harzstark, ...T. Choueiri, *IND* **2014**, *32*, 178-187.; b) R. Yazdian-Robati, P. Bayat, F. Oroojalian, M. Zargari, M. Ramezani, S. M. Taghdisi, K. Abnous, *Int. J. Biol. Macromol.* **2019**, an update review.
- (11) a) R. F. Macaya, P. Schultze, F. W. Smith, J. A. Roe, J. Feigon, *Proc. Natl. Acad. Sci.* **1993**, *90*, 3745-3749.; b) P. Schultze, R. F. Macaya, J. Feigon, *J. Mol. Biol.* **1994**, *235*, 1532-1547.
- (12) a) C. T. Griffin, Y. Srinivasan, Y. W. Zheng, W. Huang, S. R. Coughlin, *Science* **2001**, *293*, 1666-1670.; b) K. E. Brummel, S. G. Paradis, S. Butenas, K. G. Mann, *J. Am. Soc. Hematol. Blood* **2002**, *100*, 148-152.; c) S. J. Yeon, K. H. Shim, J. S. Hong, H. S. Shin, *Kor. J. Chem. Eng.* **2017**, *34*, 781-786.

- (13) a) E. R. Wang, H. Wu, Y. Niu, J. Cai, *Curr. Med. Chem.* **2011**, *18*, 4126-4138.; b) J. Lietard, H. Abou Assi, I. Gomez-Pinto, C. González, M. M. Somoza, M. J. Damha, *Nucleic acids Res.* **2017**, *45*, 1619-1632.; c) W. Kotkowiak, J. Lisowiec-Wachnicka, J. Grynda, R. Kierzek, J. Wengel, A. Pasternak, *Mol. Ther. Nucleic Acids* **2018**, *10*, 304-316.
- (14) a) G. X. He, S. H. Krawczyk, S. Swaminathan, R. G. Shea, J. P. Dougherty, T. Terhorst, ... N. Bischofberger, *J. Med. Chem.* **1998**, *41*, 2234-2242.; b) C. G. Peng, M. J. Damha, *Nucleic acids Res.* **2007**, *35*, 4977-4988.; c) A. Avino, C. Fabrega, M. Tintore, R. Eritja, *Curr. Pharm. Design* **2012**, *18*, 2036-2047.
- (15) S. Mendelboum Raviv, A. Horvath, J. Aradi, Z. Bagoly, F. Fazakas, Z. Batta, ... J. Harsfalvi, *J. Thromb. Haemost.* **2008**, *6*, 1764-1771.
- (16) R. Dolot, C. H. Lam, M. Sierant, Q. Zhao, F. W. Liu, B. Nawrot, ... X. Yang, *Nucleic Acids Res.* **2018**, *46*, 4819-4830.
- (17) I. Smirnov, N. Kolganova, R. Troisi, F. Sica, E. Timofeev, *Mol. Ther. Nucl. Acids* **2021**, *23*, 863-871.
- (18) J. H. Yum, S. Park, R. Hiraga, I. Okamura, S. Notsu, H. Sugiyama, *Org. Biomol. Chem.* **2019**, *17*, 2548-2553.
- (19) S. Park, H. Matsui, K. Fukumoto, J. H. Yum, H. Sugiyama, *RSC Adv.* **2020**, *10*, 9717-9722.
- (20) K. Murayama, Y. Tanaka, T. Toda, H. Kashida, H. Asanuma, *Chem. Eur. J.* **2013**, *19*, 14151-14158.

(21) We carefully selected seven different amino acid moieties based on the synthetic issue and its side chain characteristics such as side chain bulkiness (Ala vs Trp), hydrophilic side chain (Lys/Gln/His) and hydrophobic side chain (Phe/Trp/Met). ANHs used in this study could be readily incorporated into oligonucleotides by solid-phase DNA synthesis without additional protection.

(22) a) K. A. I. L. L. A. T. H. E. Padmanabhan, K. P. Padmanabhan, J. D. Ferrara, J. E. Sadler, A. Tulinsky, *J. Biol. Chem.* **1993**, *268*, 17651-17654.; b) S. Nagatoishi, N. Isono, K. Tsumoto, N. Sugimoto, *Biochim.* **2011**, *93*, 1231-1238.

(23) a) R. D. Langdell, R. H. Wagner, K. M. Brinkhous, *J. Lab. Clinic. Med.* **1953**, *41*, 637-647.;
b) H. L. Bao, T. Ishizuka, A. Yamashita, E. Furukoji, Y. Asada, Y. Xu, **2020**, *J. Med. Chem.*,
DOI: 10.1021/acs.jmedchem.0c01711

(24) a) T. J. Rydel, K. G. Ravichandran, A. Tulinsky, W. Bode, R. Huber, C. Roitsch, J. W. Fenton, *Science* **1990**, *249*, 277-280.; b) J. A. Huntington, *J. Thromb. Haemost.* **2005**, *3*, 1861-1872.

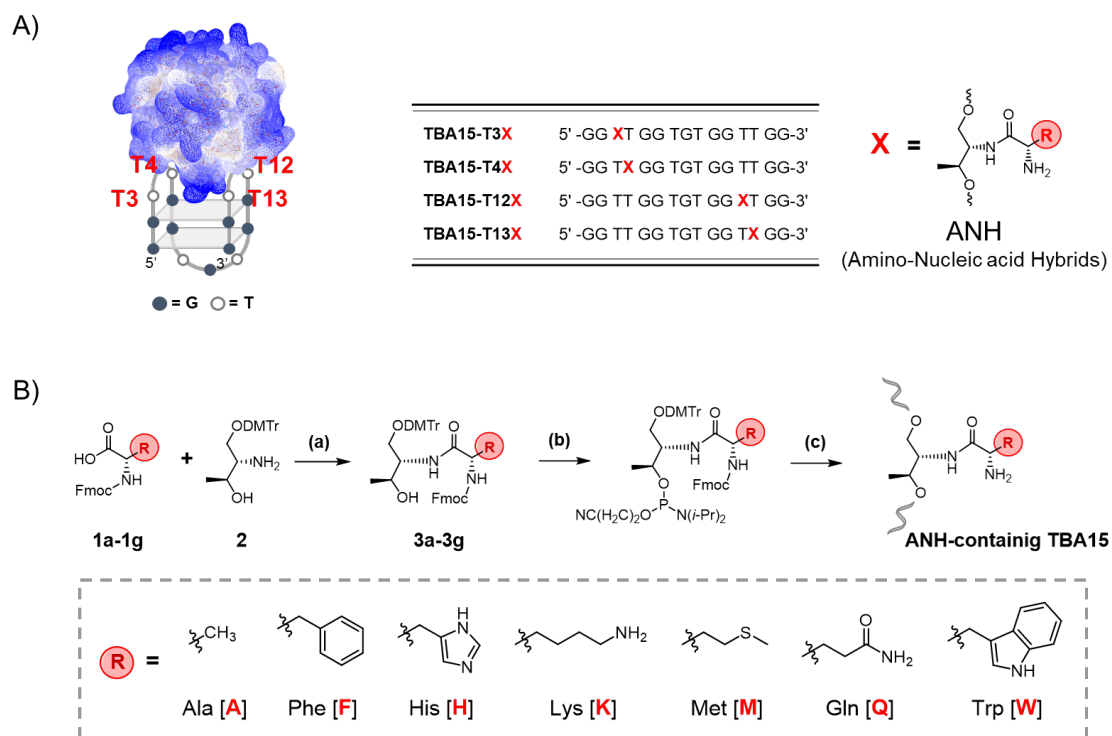


Figure 1. Synthesis of ANHs-containing TBA15 library. (A) TB and TBA sequence functionalized with amino-nucleic acid hybrids (ANHs), (B) Synthetic scheme of ANHs and amino acid conjugates using in this study

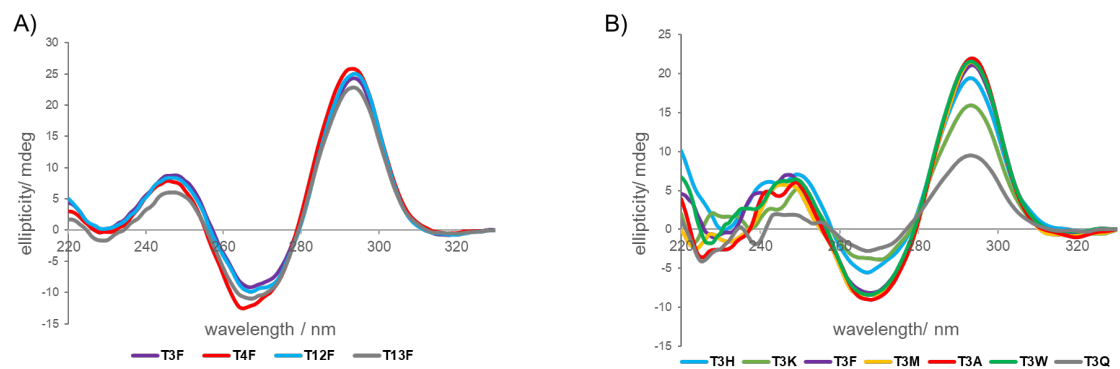


Figure 2. CD spectra of various ANH-modified TBA15 (A) CD spectra of Phe-ANH containing TBA15, (B) CD spectra of various ANH-modified TBA15

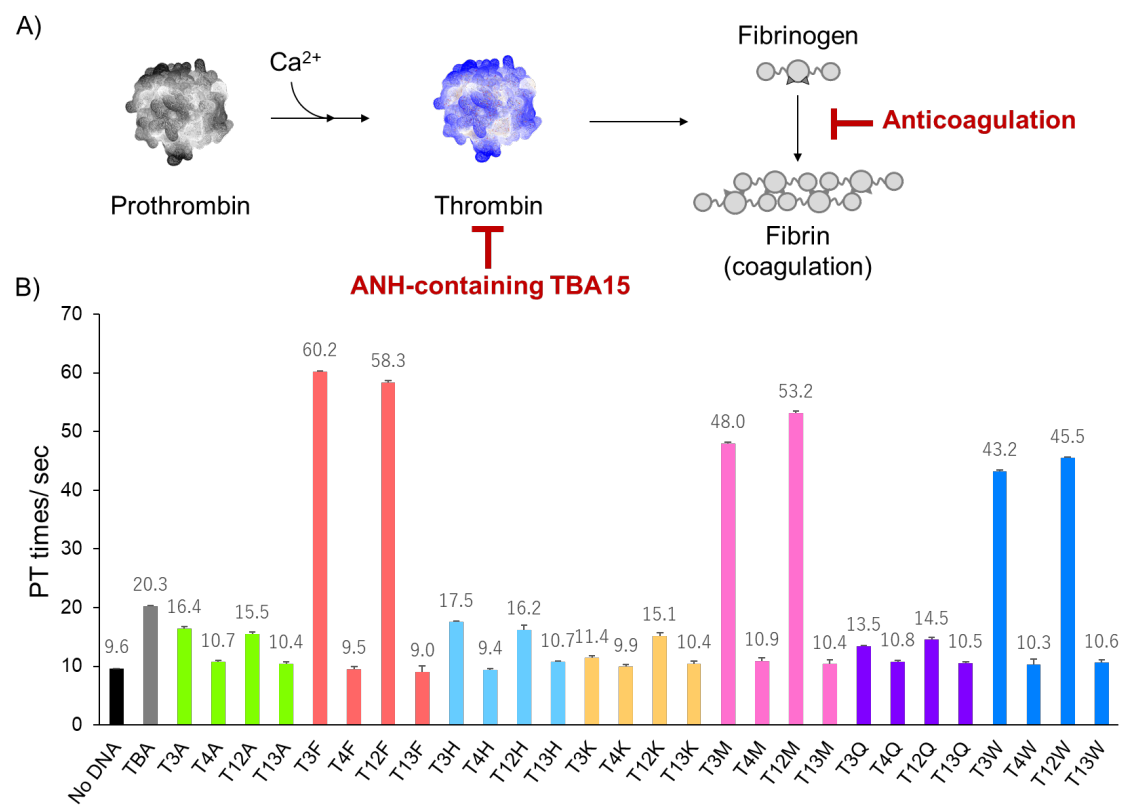


Figure 3. PT assay results with native- and ANHs-containing TBA15 DNA aptamers. (A) Schematic illustration of PT assay, (B) Comparison of PT results

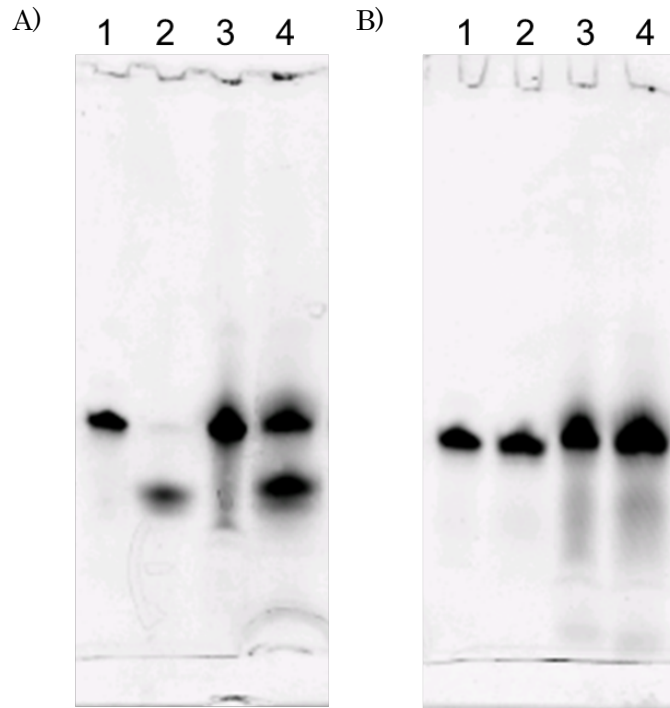


Figure 4. Gel image of the endonuclease DNase I treated native and T3F TBA sequences

(A) Denaturing PAGE image of the native and T3F TBA sequences in the absence of 100 mM KCl (lane 1: native TBA before DNase I treatment, lane 2: native TBA after DNase I treatment, lane 3: T3F TBA before DNase I treatment, and lane 4: T3F TBA after DNase I treatment), (B) Denaturing PAGE image of the native and T3F TBA sequences in the presence of 100 mM KCl (lane 1: native TBA before DNase I treatment, lane 2: native TBA after DNase I treatment, lane 3: T3F TBA before DNase I treatment, and lane 4: T3F TBA after DNase I treatment). Solution conditions: 1 μ M each DNA and 10 unit of endonuclease DNase I in 1X work buffer () in the presence/absence of 100 mM KCl

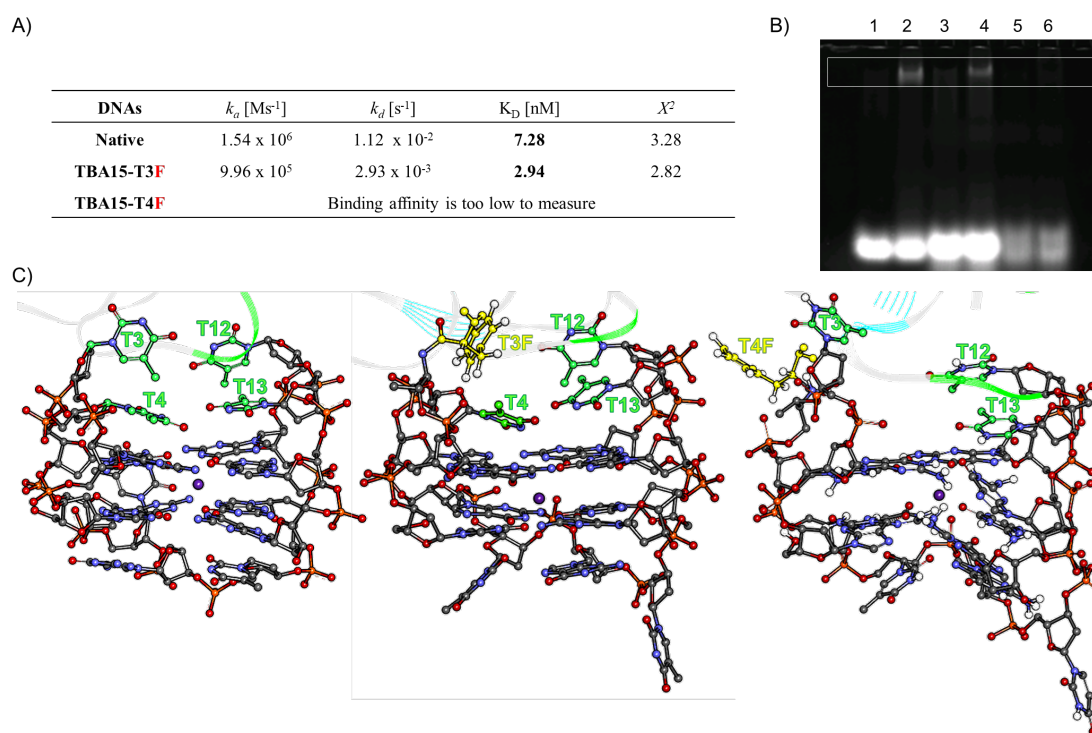


Figure 5. Investigation of binding affinities with T3F and T4F DNA. (A) Quantitative binding affinities by SPR assay, (B) TB binding assay by EMSA, (C) Molecular modeling results.

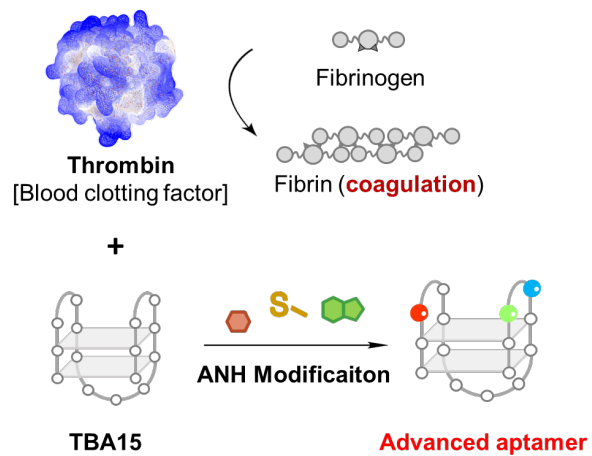
(A) For SPR assay, the biotinylated DNA is immobilized to the chip to obtain the desired immobilization level (approximately 100 RU rise). A series of thrombin solutions with various concentrations were prepared in the HBS-EP buffer with 100 mM KCl and injected. The predefined models (1:1 binding model with mass transfer or with drafting baseline) were used for fitting the sensorgrams of TB to give better fitting. (B) Native PAGE image of the native and T3F/T4F TBA sequences in the presence of 100 mM KCl (lane 1: native TBA, lane 2: native TBA with 1 equiv. of thrombin, lane 3: T3F TBA, lane 4: T3F TBA with 1 equiv. of thrombin, lane 5: T4F TBA, and lane 6: T4F TBA with 1 equiv. of thrombin), (C) Molecular modeling, energy minimization, and MD were performed with Discovery Studio Client 2019 software package. See SI for the details.

Graphical Abstract

<Title> **Systematic Approach to DNA Aptamer Design Using Amino Acid–Nucleic Acid Hybrids (ANHs) Targeting Thrombin**

<Authors' names> *Ji Hye Yum, Takumi Ishizuka, Koyuki Fukumoto, Daisuke Hori, Hong-Liang Bao, Yan Xu, Hiroshi Sugiyama*, and Soyoung Park**

<Diagram>



Supporting Information

Systematic DNA Aptamer Design Approach with Amino Acid-Nucleic Acid Hybrids (ANHs) Targeting Thrombin

Ji Hye Yum^{1,‡}, Takumi Ishizuka^{3,‡}, Koyuki Fukumoto¹, Daisuke Hori¹, Hong-Liang Bao³, Yan Xu³, Hiroshi Sugiyama^{1,2,}, and Soyoung Park^{1,*}*

¹Department of Chemistry, Graduate School of Science, Kyoto University, Kitashirakawa-oiwakecho, Sakyo-ku, Kyoto 606-8502, Japan

²Institute for Integrated Cell-Material Sciences (iCeMS), Kyoto University, Yoshida-ushinomiyacho, Sakyo-ku, Kyoto 606-8501, Japan

³Division of Chemistry, Department of Medical Sciences, Faculty of Medicine, University of Miyazaki, 5200 Kihara, Kiyotake, Miyazaki 889-1692, Japan

**Corresponding author:* Dr. Soyoung Park, Prof. Dr. Hiroshi Sugiyama

Tel.: (+)81-75-753-4002; Fax: (+)81-75-753-3670

E-mail: oleesy@kuchem.kyoto-u.ac.jp, hs@kuchem.kyoto-u.ac.jp (H.S.)

Table of Contents

Materials	3
Methods and Equipment	4
Synthesis and characterization of ANHs products	5
Scheme S1. Synthetic Route of Amino-Nucleic Acids Hybrids(ANHs).....	5
Figure S1. Methionine-conjugated D-threoninol backbone (3e)	5
Figure S2. Glutamine-conjugated D-threoninol backbone (3f)	7
Figure S3. Tryptophan-conjugated D-threoninol backbone (3g).....	7
Oligonucleotide (ODN) Synthesis	8
Table S1. Analytical HPLC profile of synthesized ODNs	10
Table S2. MALDI-TOF-Mass data of ODNs.....	11
Table S3. Sequences of native ODNs	12
Prothrombin time measurement	13
Table S4. Comparison with previous studies or modified TBA variants.....	15
CD Spectroscopy	16
Figure S4. CD spectrum of the native TBA sequence ^a	16
Figure S5. CD spectra of Phe-ANH containing TBA sequences in the presence/absence of TB ^a	17
Figure S6. CD spectra of various ANHs-modified TBA sequence ^a	18
UV-Melting	19
Figure S7. T _m values and UV-melting curves of Phe-ANH containing TBA sequences ^a ...	20
Figure S8. T _m values of various ANH-modified TBA sequences ^a	21
Nuclease resistance experiments	22
EMSA	22

SPR assays	23
Figure S9. SPR sensorgrams with the native and Phe-ANH containing TBA sequences ^a	24
Molecular Modeling Study	25
Figure S10. The results of Phe-ANH containing TBA15 after several minimization.....	26
Figure S11. Molecular dynamic results of the native, T3F, and T4F TBA with TB	27
References	27

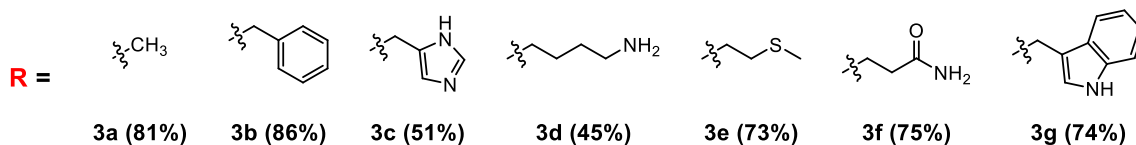
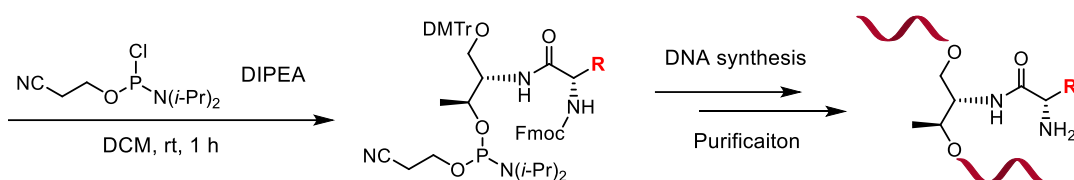
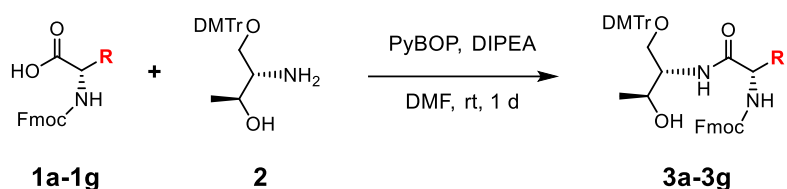
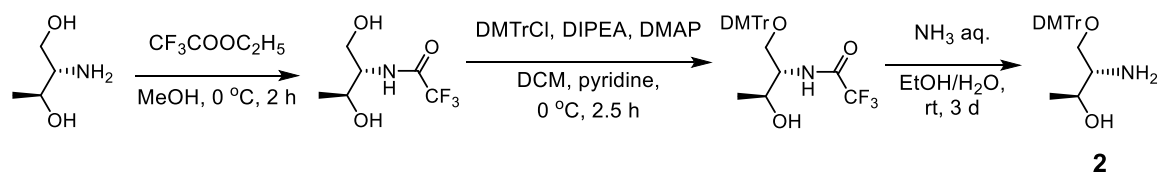
Materials

N,N-Diisopropylethylamine, *N,N*-Dimethylformamide, trimethylamine was received from Nacalai tesque Co. and used as received. 4,4'-Dimethoxytrityl chloride, *N,N*-diisopropylchloro phosphoramidite, Potassium carbonate, DNase I (RNase free) were bought from Wako chemicals and used without further purification. D-threoninol (97%), Fmoc-Ala-OH (>97%), Fmoc-Phe-OH (>97%), Fmoc-His-OH, Fmoc-Lys-OH, Fmoc-Met-OH, Fmoc-Gly-OH, Fmoc-Trp-OH, and thromboplastin reagent were purchased from Sigma-Aldrich Chemicals Co. and used as received. PyBOP was received from Novabiochem and used without further purification. Ethyl trifluoroacetate was obtained from TCI. Glen-Pak™ DNA and RNA cartridges columns were purchased at Glen Research. Synthetic oligonucleotides not containing ANHs were obtained from Sigma Genosys. Water was deionized (specific resistance of ≥ 18.0 MW cm at 25°C) by a Milli-Q system (Millipore Corp.). All reactions were carried out under an argon atmosphere unless otherwise stated.

Methods and Equipment

NMR spectra were obtained on a JEOL JNM ECA-600 spectrometer operating at 600 MHz for ^1H NMR and 150 MHz for ^{13}C NMR in CDCl_3 unless otherwise noted. Flash column chromatography was performed employing Silica Gel 60 (70–230 mesh, Merck Chemicals). Silica-gel preparative thin-layer chromatography (PTLC) was performed using plates from Silica gel 70 PF₂₅₄ (Wako Pure Chemical Ind. Ltd.). DNA concentrations were measured by NanoDrop ND-1000 spectrophotometer. Stock 100 mM Tris-HCl (pH 7.5) and 100 mM PBS (pH 7.8) buffers were prepared by dissolving sodium cacodylate trihydrate (1.07 g, 5.0 mmol) in milliQ water (25 mL) before adjusting to the desired pH with hydrochloric acid and minimal sodium hydroxide, then topping up to 50 mL with milliQ water. Measurement of pH was conducted with a LAQUA F-72 pH/ion meter (HORIBA Ltd., Kyoto, Japan). SPR assays were performed with a Biacore X system (GE Healthcare), and processing of data was carried out by using BIA evaluation, version 3.2. Prothrombin time measurements were conducted with Thrombotrack produced from Sanko Junyaku Co. Ltd. Molecular modeling, energy minimization, and molecular dynamics were carried out with BIOVIA Discovery Studio 2020 software packs.

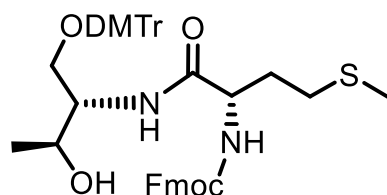
Synthesis and characterization of ANHs products



Scheme S1. Synthetic Route of Amino-Nucleic Acids Hybrids(ANHs)

Reagents and conditions: (a) $\text{CF}_3\text{COOC}_2\text{H}_5$, dry MeOH, 0°C , 2 h ; (b) DMT-Cl, DIEA, DMAP, CH_2Cl_2 , pyridine, $0^\circ\text{C} \rightarrow \text{r.t.}$ 2.5 h; (c) NH_3 , EtOH/ H_2O , r.t. 3 days ; (d) PyBOP, DIEA, DMF, r.t., 1 day. ; (e) $(i\text{Pr}_2\text{N})_2\text{PO}(\text{CH}_2)_2\text{CN}$, DIEA, CH_3CN , $0^\circ\text{C} \rightarrow \text{r.t.}$ 1.5 h

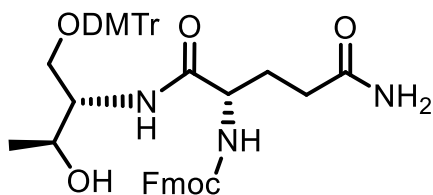
Figure S1. Methionine-conjugated D-threoninol backbone (3e)



(9H-fluoren-9-yl)methyl ((S)-1-(((2S,3S)-1-(bis(4-methoxyphenyl)(phenyl)methoxy)-3-hydroxybutan-2-yl)amino)-4-(methylthio)-1-oxobutan-2-yl)carbamate

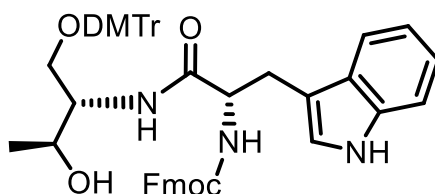
Detail synthetic route for DMTr-protected Dthreoninol backbone (**1**) is written on the previous report by Asanuma, H. and his co-workers.^{S1} And the synthetic scheme and the characterization of compound **3a-3d** have been reported on our previous literature.^{S2} To DMF solution (20 mL) containing Fmoc-Met-OH (mg, 1.0 mmol), PyBOP (520 mg, 1.0 mmol), and DIEA (0.7 mL) was added DMF solution (5 mL) of compound **1** (489 mg, 1.2 mmol). Then the resulting reaction mixture was stirred at room temperature for 1 day. After the precipitate was removed by filtration, the filtrate was evaporated and the obtained solid was subjected to silica gel column chromatography (EtOAc Hex = 2:1) to afford 555 mg (0.73 mmol) of the product (yield, 73%).

¹H NMR ((CD₃)₂CO): δ 7.85 (d, J = 7.7 Hz, 2H), 7.70 (d, J = 7.1 Hz, 1H), 7.61 (d, J = 7.7 Hz, 1H), 7.46 (d, J = 7.7 Hz, 2H), 7.41-7.38 (m, 2H), 7.33-7.27 (m, 9H), 7.18 (q, J = 8.5 Hz, 2H), 6.85 (d, J = 8.9 Hz, 4H), 4.43 (td, J = 8.0, 5.3 Hz, 1H), 4.30 (d, J = 7.7 Hz, 2H), 4.19 (t, J = 7.4 Hz, 1H), 4.11-4.09 (m, 1H), 4.06-4.02 (m, 1H), 3.84 (d, J = 4.8 Hz, 1H), 3.73 (d, J = 3.6 Hz, 6H), 3.26 (dd, J = 8.9, 5.9 Hz, 1H), 3.12 (dd, J = 8.9, 5.9 Hz, 1H), 2.63-2.56 (m, 2H), 2.20-2.14 (m, 1H), 2.06-2.04 (m, 3H), 2.03-1.97 (m, 1H), 1.08 (d, J = 6.5 Hz, 3H). ¹³C NMR ((CD₃)₂CO): d 171.93, 159.13, 156.72, 145.91, 144.87, 144.45, 141.70, 136.59, 130.55, 128.61, 128.20, 127.60, 127.06, 125.87, 125.74, 120.41, 113.49, 86.38, 66.95, 66.50, 64.06, 55.08, 47.62, 32.83, 20.49, 14.86. HRMS (ESI-TOF) calculated for C₄₅H₄₈N₂NaO₇S [M+Na]⁺ 783.9358, found 783.3074.

Figure S2. Glutamine-conjugated D-threoninol backbone (3f)

(9H-fluoren-9-yl)methyl ((S)-5-amino-1-(((2S,3S)-1-(bis(4-methoxyphenyl)(phenyl)methoxy)-3-hydroxybutan-2-yl)amino)-1,5-dioxopentan-2-yl)carbamate

^1H NMR ($(\text{CD}_3)_2\text{CO}$): δ 7.86 (d, $J = 7.7$ Hz, 2H), 7.72 (d, $J = 6.5$ Hz, 1H), 7.64 (d, $J = 7.7$ Hz, 1H), 7.46 (d, $J = 7.7$ Hz, 2H), 7.41-7.38 (m, 2H), 7.34-7.28 (m, 9H), 7.17 (t, $J = 6.8$ Hz, 1H), 7.02 (d, $J = 7.1$ Hz, 1H), 6.90 (br, NH), 6.86 (d, $J = 7.7$ Hz, 4H), 6.28 (br, NH_2), 4.29-4.20 (m, 4H), 4.08 (s, 1H), 4.01 (d, $J = 4.2$ Hz, 1H), 3.69 (s, OH), 3.74 (d, $J = 4.2$ Hz, 6H), 3.27 (dd, $J = 8.8, 4.9$ Hz, 1H), 3.11 (dd, $J = 8.9, 5.9$ Hz, 1H), 2.38 (t, $J = 7.1$ Hz, 2H), 2.14 (q, $J = 6.5$ Hz, 1H), 2.08-2.04 (m, 1H), 1.08 (d, $J = 5.9$ Hz, 3H). ^{13}C NMR ($(\text{CD}_3)_2\text{CO}$): δ 174.91, 172.14, 159.18, 156.82, 145.97, 144.94, 144.55, 141.75, 136.62, 130.61, 128.68, 128.24, 127.47, 127.10, 126.02, 125.86, 120.45, 113.54, 86.40, 67.08, 66.73, 64.18, 55.66, 55.12, 47.65, 32.08, 20.45. HRMS (ESI-TOF) calculated for $\text{C}_{45}\text{H}_{47}\text{N}_3\text{NaO}_8$ $[\text{M}+\text{Na}]^+$ 780.8738, found 780.3251.

Figure S3. Tryptophan-conjugated D-threoninol backbone (3g)

(9H-fluoren-9-yl)methyl ((S)-1-(((2S,3S)-1-(bis(4-methoxyphenyl)(phenyl)methoxy)-3-hydroxybutan-2-yl)amino)-3-(1H-indol-3-yl)-1-oxopropan-2-yl)carbamate

^1H NMR ($(\text{CD}_3)_2\text{CO}$): δ 10.06 (s, NH), 7.83 (d, $J = 7.8$ Hz, 2H), 7.68 (d, $J = 8.3$ Hz, 1H), 7.61 (d, $J = 7.7$ Hz, 1H), 7.53 (d, $J = 7.7$ Hz, 1H), 7.46 (d, $J = 7.7$ Hz, 2H), 7.37 (t, $J = 7.1$ Hz, 3H), 7.32-7.23 (m, 9H), 7.17 (t, $J = 7.4$ Hz, 1H), 7.09 (t, $J = 7.4$ Hz, 1H), 6.99 (t, $J = 7.1$ Hz, 1H), 6.85 (d, $J = 7.1$ Hz, 4H), 6.73 (d, $J = 8.3$ Hz, NH), 4.62 (dd, $J = 13.7, 7.7$ Hz, 1H), 4.20 (t, $J = 7.7$ Hz, 2H), 4.12 (t, $J = 7.1$ Hz, 1H), 4.06 (d, $J = 7.7$ Hz, 1H), 4.04 (d, $J = 7.7$ Hz, 1H), 3.78 (t, $J = 2.7$ Hz, OH), 3.73 (d, $J = 3.0$ Hz, 6H), 3.38 (dd, $J = 14.2, 5.3$ Hz, 1H), 3.23 (dd, $J = 8.9, 6.5$ Hz, 1H), 3.14-3.09 (m, 2H), 1.00 (d, $J = 6.5$ Hz, 3H). ^{13}C NMR ($(\text{CD}_3)_2\text{CO}$): d 172.31, 159.17, 156.62, 145.99, 144.83, 144.56, 141.69, 137.31, 136.69, 130.61, 128.68, 128.23, 128.15, 127.63, 127.09, 125.92, 125.56, 124.10, 121.81, 120.39, 119.26, 119.12, 113.52, 111.84, 111.29, 86.41, 67.01, 66.45, 63.88, 55.12, 47.60, 26.69, 20.33. HRMS (ESI-TOF) calculated for $\text{C}_{51}\text{H}_{49}\text{N}_3\text{NaO}_7$ $[\text{M}+\text{Na}]^+$ 838.9568, found 838.3455.

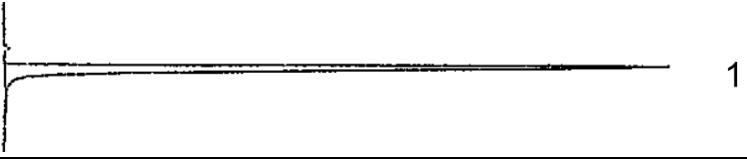
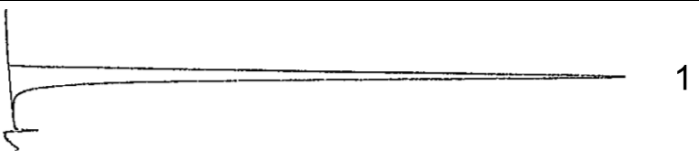

Oligonucleotide (ODN) Synthesis

ODNs were synthesized on solid supports using various ANHs product phosphoramidite (compound **3a-3g**) and commercially available O^5' -dimethoxytrityl $-2'$ -deoxyribonucleoside O^3' -phosphoramidites. Compound **3a-3g** was prepared by dropwise addition of DIPEA at 0°C to a solution of compound **3a-3g** in CH_2Cl_2 followed by stirring at 0°C for 10 min.

Phosphoramidochloridous acid was subsequently added and the mixture was stirred for a further 10 min at 0 °C before warming to room temperature and stirring for another 1 h. After removal of the solvent, the residue was dissolved in MeCN and used immediately without purification for solid-phase DNA synthesis. Solid-phase oligonucleotide synthesis was performed on an ABI DNA synthesizer (Applied Biosystem, Foster City, CA) or M-2-MX DNA/RNA synthesizer (Nihon Techno Service Co., Ltd., Tsukuba, Japan). The modified phosphoramidite was chemically synthesized as described above and without purification incorporated into oligonucleotide through coupling reaction for 10 minutes. The coupling yields of ANHs phosphoramidites were around 10 % less than the ones obtained with standard phosphoramidite building blocks. Cleavage from the solid support and deprotection were accomplished with 50:50 of MeNH₂ in 40 wt. % in water and NH₃ in 28 wt. % in water at RT for 15 min and then at 65 °C for 15 min. The synthesized oligonucleotides were eluted from Glen-Pak™ DNA purification cartridges with purification steps are performed as per procedure. The final elution was subjected to normal-phase HPLC purification (2 % to 40 % ACN in 50 mM TEAA (pH 7.0) buffer, flow rate of 3.0 mL/min). After purification by HPLC, the products were confirmed by MALDI-TOF MS using a Bruker microflex-KSII (Bruker Corporation, Billerica, MA) (Table S2). DNA concentrations were determined by using NanoDrop ND-1000 (NanoDrop Technologies, Wilmington, DE).

For HPLC analysis, COSMOSIL 5C18 AR-II (Nacalai Tesque, Inc., Kyoto, 150 × 10 mm id), a linear gradient of 2 % to 30 % acetonitrile (in 50 mM TEAA (pH 7.0) buffer) over 30 min at a flow rate of 3.0 mL/min and detection at 254 nm were used.

Table S1. Analytical HPLC profile of synthesized ODNs

ODN	HPLC Profile
TBA15-T3 A	10.333  1
TBA15-T3 F	9.258  1
TBA15-T3 H	19.617  1

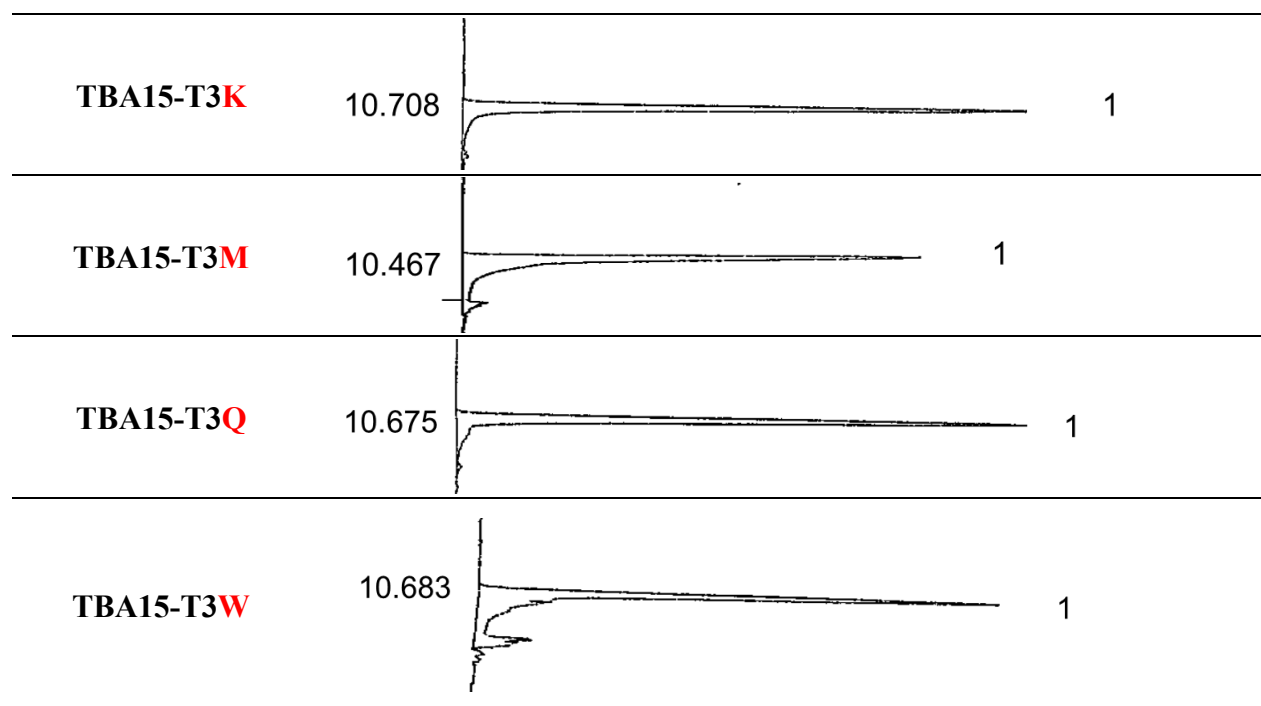


Table S2. MALDI-TOF-Mass data of ODNs

Name	DNA oligomers	Calcd.	Found
TBA-T3A	5'-GG AT GG TGT GG TT GG-3'	4660.04	4662.34
TBA-T4A	5'-GG TA GG TGT GG TT GG-3'	4660.04	4662.34
TBA-T12A	5'-GG TT GG TGT GG AT GG-3'	4660.04	4661.97
TBA-T13A	5'-GG TT GG TGT GG TA GG-3'	4660.04	4665.32
TBA-T3F	5'-GG FT GG TGT GG TT GG-3'	4736.16	4736.53
TBA-T4F	5'-GG TF GG TGT GG TT GG-3'	4736.16	4736.46
TBA-T12F	5'-GG TT GG TGT GG FT GG-3'	4736.16	4734.48
TBA-T13F	5'-GG TT GG TGT GG TF GG-3'	4736.16	4735.99

TBA-T3H	5'-GG HT GG TGT GG TT GG-3'	4726.13	4729.56
TBA-T4H	5'-GG TH GG TGT GG TT GG-3'	4726.13	4727.88
TBA-T12H	5'-GG TT GG TGT GG HT GG-3'	4726.13	4729.42
TBA-T13H	5'-GG TT GG TGT GG TH GG-3'	4726.13	4730.12
TBA-T3K	5'-GG KT GG TGT GG TT GG-3'	4717.16	4720.34
TBA-T4K	5'-GG TK GG TGT GG TT GG-3'	4717.16	4720.49
TBA-T12K	5'-GG TT GG TGT GG KT GG-3'	4717.16	4718.68
TBA-T13K	5'-GG TT GG TGT GG TK GG-3'	4717.16	4720.58
TBA-T3M	5'-GG MT GG TGT GG TT GG-3'	4720.14	4719.76
TBA-T4M	5'-GG TM GG TGT GG TT GG-3'	4720.14	4720.27
TBA-T12M	5'-GG TT GG TGT GG MT GG-3'	4720.14	4718.89
TBA-T13M	5'-GG TT GG TGT GG TM GG-3'	4720.14	4720.58
TBA-T3Q	5'-GG QT GG TGT GG TT GG-3'	4717.08	4719.63
TBA-T4Q	5'-GG TQ GG TGT GG TT GG-3'	4717.08	4720.22
TBA-T12Q	5'-GG TT GG TGT GG QT GG-3'	4717.08	4719.98
TBA-T13Q	5'-GG TT GG TGT GG TQ GG-3'	4717.08	4717.63
TBA-T3W	5'-GG WT GG TGT GG TT GG-3'	4775.16	4776.36
TBA-T4W	5'-GG TW GG TGT GG TT GG-3'	4775.16	4777.12
TBA-T12W	5'-GG TT GG TGT GG WT GG-3'	4775.16	4778.89
TBA-T13W	5'-GG TT GG TGT GG TW GG-3'	4775.16	4775.99
T3F-FAM	5'- FAM -GG FT GG TGT GG TT GG-3'	5471.89	5467.27
T4F-FAM	5'- FAM -GG TF GG TGT GG TT GG-3'	5471.89	5465.74
T3F-Biotin	5'- Bio -GG FT GG TGT GG TT GG-3'	5171.64	5148.95
T4F-Biotin	5'- Bio -GG TF GG TGT GG TT GG-3'	5171.64	5142.09

Native DNA oligomers (TBA15, TBA15-FAM, TBA15-Biotin) were purchased from Sigma Genosys.

Table S3. Sequences of native ODNs

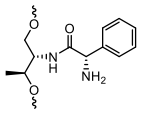
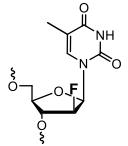
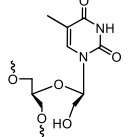
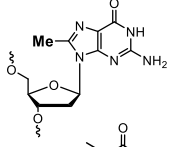
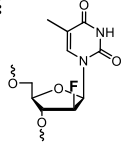
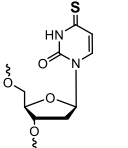
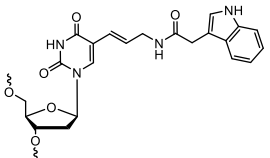
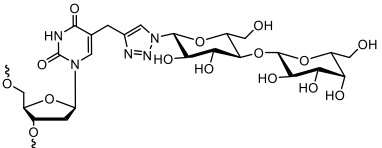
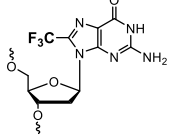
Name	Sequence
TBA15	5'-GG TT GG TGT GG TT GG-3'
TBA15-FAM	5'- FAM -GG TT GG TGT GG TT GG-3'
TBA15-Biotin	5'- Bio -GG TT GG TGT GG TT GG-3'

Prothrombin time measurement

Samples were prepared by heating the oligonucleotides at 95 °C for 5 min and gradually cooling to room temperature. Annealing solutions (100 μ M) were obtained in 100 mM KCl and 10 mM potassium phosphate buffer (pH 7.0). Prothrombin time experiment was performed by using Thrombotrack (Sanko Junyaku Co., Ltd.). Human plasma (100 μ L) and 3 μ L of natural or modified

TBA sequences were incubated at 37 °C for 1 min. Then, 200 µL of thromboplastin reagent was added. The final concentration of natural or modified TBA is 1 µM. The prothrombin time measurement was carried out in triplicate. All data are presented as the means and standard deviation. Differences between control and modified TBAs were tested using the one-way analysis of variance with Dunnett's multiple comparison test (GraphPad Prism 5, GraphPad Software, Inc., San Diego, CA, USA).

Table S4. Comparison with previous studies or modified TBA variants

ref	modifications	modification positions	ΔT_m	relative PT time	K_d
This work		T3	1.9	3	2.5-folds
13b		T3	7.2	-	3-folds
13c		T7	3.5	0.94	1-fold
14a		G1, G3, G10, G14	-	1.6	-
14b		T3, T4, T7, T9	0.9	-	4-folds
15		T3, T7, T9, T13	-	0.35	-
16		T4	0.3	-	2.8-fold
17		T3	0.8	1.1	2-folds
23b		G14	7.6	1.5	-

CD Spectroscopy

CD spectra of oligonucleotide solutions collected in 1 nm steps from 360 nm or 320 nm to 220 nm were measured using JASCO J-805LST Spectrometer in a 1 cm quartz cuvette. Each spectrum shown is the average of two individual scans. The samples were denatured at 95 °C for 5 min and annealed slowly to RT until experiments were initiated. All melting samples were prepared in a total volume of 120 μ L containing 4.0 μ M oligonucleotide and 10 mM PBS buffer (pH 7.6) with 100 mM KCl for native or ANHs-containing TBA sequences in the presence/absence of various equivalent of TB.

Figure S4. CD spectrum of the native TBA sequence ^a

^a Solution conditions: 4 μ M each DNA and 100 mM KCl in 10 mM PBS buffer (pH 7.6).

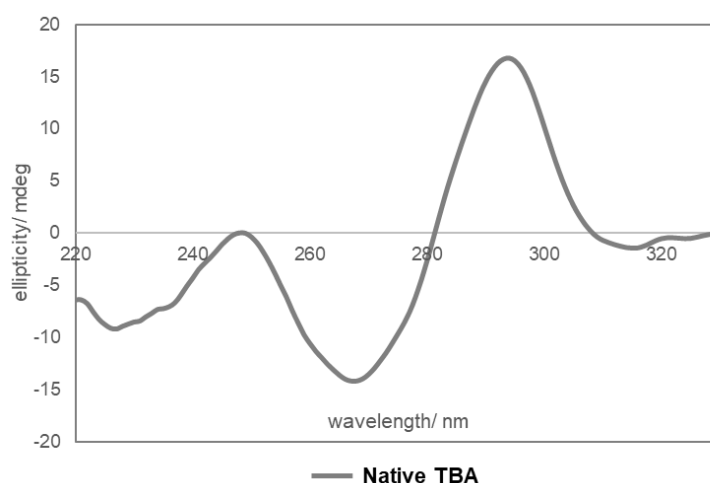
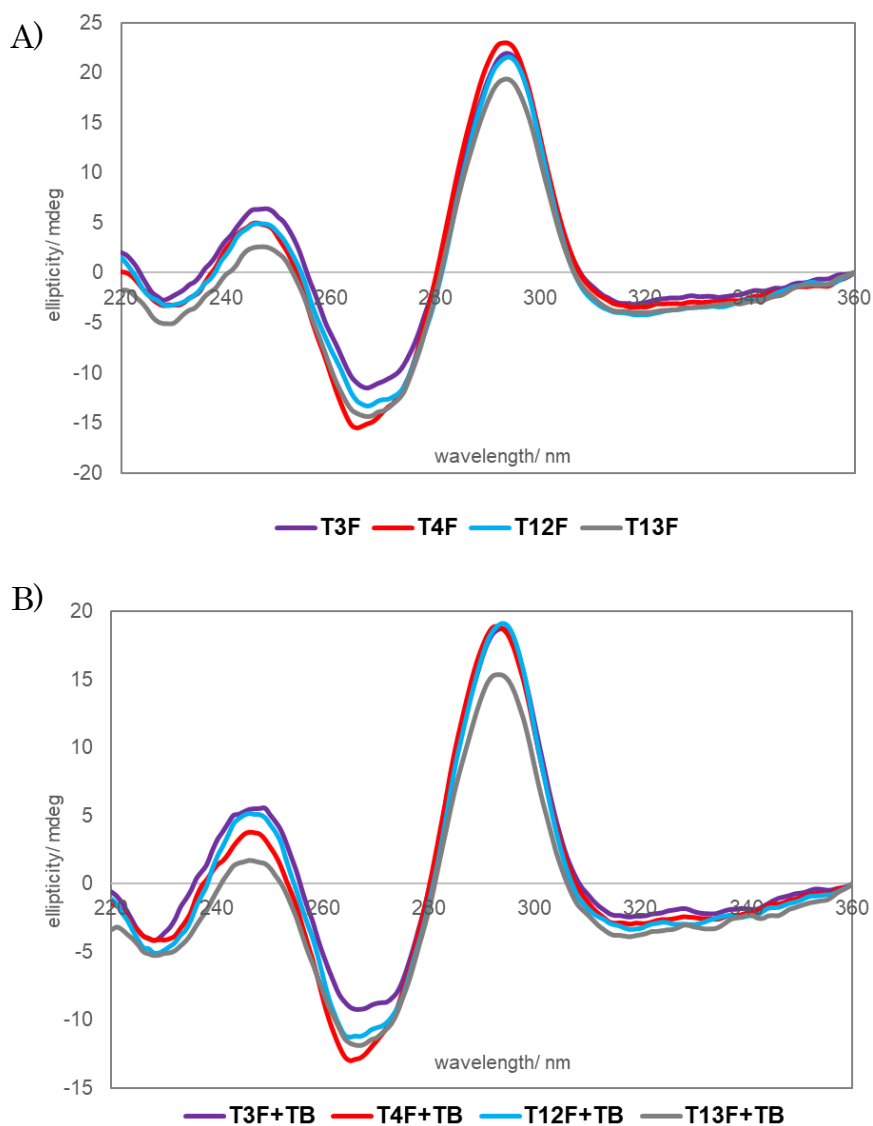
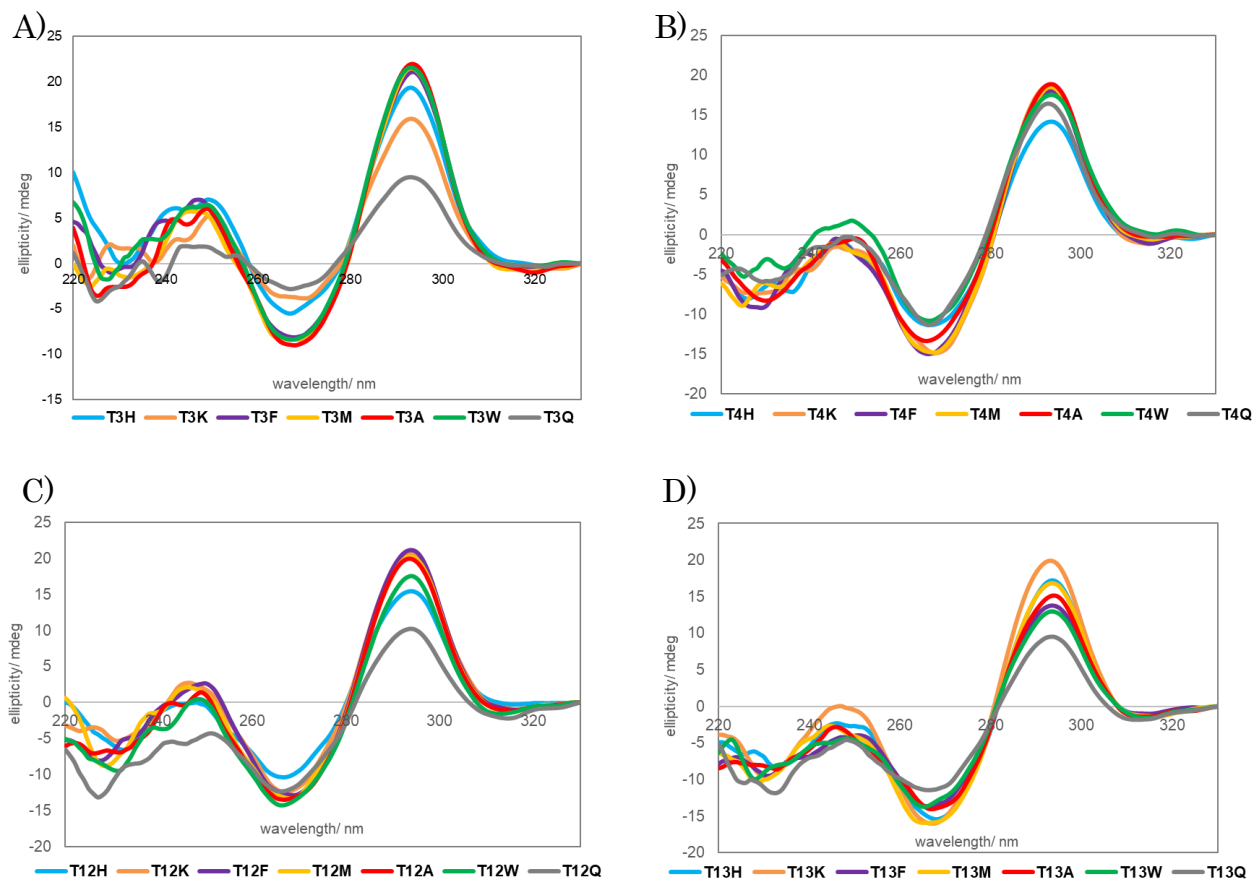


Figure S5. CD spectra of Phe-ANH containing TBA sequences in the presence/absence of TB ^a

^a Solution conditions: 4 μ M each DNA, 1.0 equiv. of TB, and 100 mM KCl in 10 mM PBS buffer (pH 7.6).



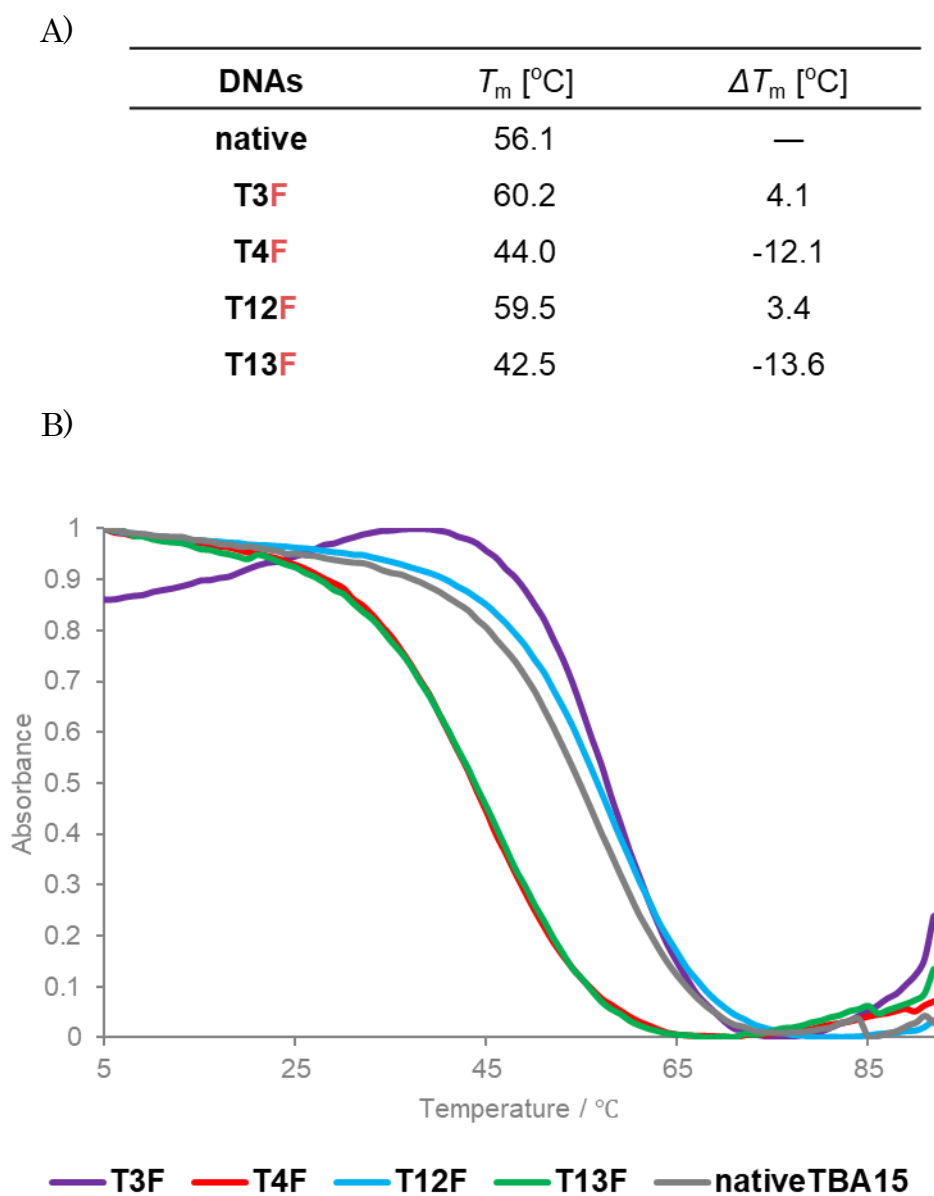
A) CD spectra of Phe-ANH containing TBA sequences in the absence of 1.0 equiv. of TB, B) CD spectra of Phe-ANH containing TBA sequences in the presence of 1.0 equiv. of TB.

Figure S6. CD spectra of various ANHs-modified TBA sequence ^a^a Solution conditions: 4 μ M each DNA and 100 mM KCl in 10 mM PBS buffer (pH 7.6).

A) CD spectra of various ANHs T3 position modified TBA sequences, B) CD spectra of various ANHs T4 position modified TBA sequences, C) CD spectra of various ANHs T12 position modified TBA sequences, D) CD spectra of various ANHs T13 position modified TBA sequences.

UV-Melting

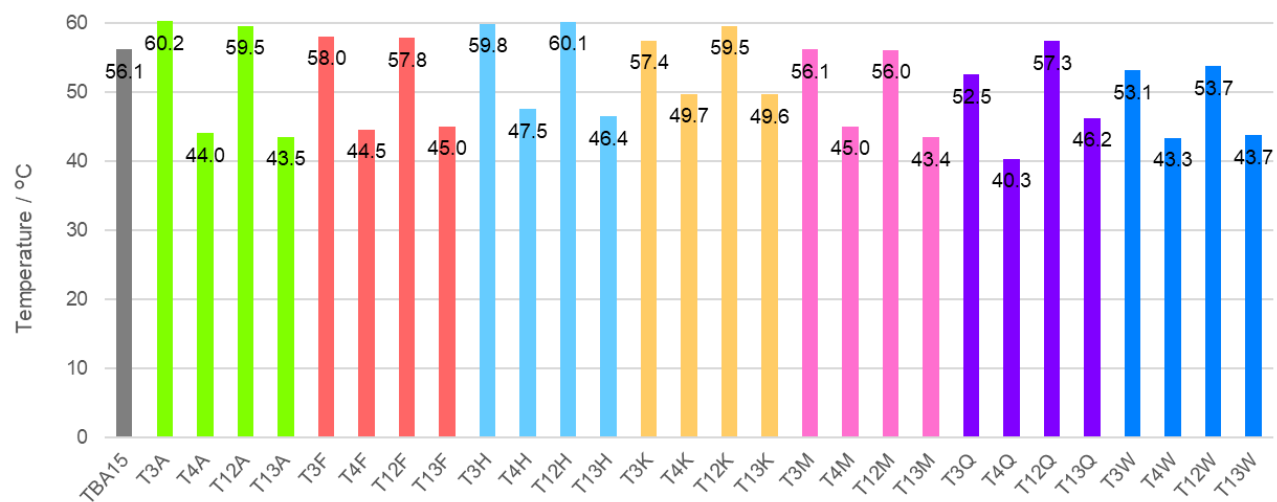
Melting temperatures were determined by measuring changes in absorbance at 295 nm as a function of temperature on a JASCO V-750 spectrophotometer equipped with a JASCO PAC-743R thermocontrolled cell changer and a JASCO CTU-100 thermocirculator. Absorbance was recorded from 15 °C to 90 °C at a rate of 1 °C/min. The melting samples were denatured at 95 °C for 5 min and annealed slowly to room temperature then stored at 4 °C until experiments were initiated. All melting samples were prepared in a total volume of 120 µL containing 10 µM oligonucleotide and 10 mM PBS buffer (pH 7.0) with 100 mM KCl for native or ANHs-containing TBA sequences.

Figure S7. T_m values and UV-melting curves of Phe-ANH containing TBA sequences ^a^a Solution conditions: 10 μ M each DNA and 100 mM KCl in 10 mM PBS buffer (pH 7.6).

A) T_m values of the native and Phe-ANH containing TBA sequences, B) UV-melting curves of the native and Phe-ANH containing TBA sequences.

Figure S8. T_m values of various ANH-modified TBA sequences ^a

^a Solution conditions: 10 μ M each DNA and 100 mM KCl in 10 mM PBS buffer (pH 7.6).



Nuclease resistance experiments

Native and Phe-ANH modified oligonucleotides were dissolved at a concentration of 1 μM in 10 μL of DNase I reaction buffer (1X) in the presence (or absence) of 100 mM KCl. Samples were heated to 95 $^{\circ}\text{C}$ and cooled down to room temperature at a rate of -1 $^{\circ}\text{C}/\text{min}$ before the enzyme treatment. Ten units of DNase I endonuclease (RNase free, Fujifilm) were added to the aptamer samples. After incubation for 30 min at 37 $^{\circ}\text{C}$, reaction mixtures were terminated by addition of 1 μL , 0.5 M EDTA solution and 5 min heat treatments (95 $^{\circ}\text{C}$). The analysis was conducted by electrophoresis in polyacrylamide gel. Electrophoresis was performed with a 20% polyacrylamide gel in 7 M urea and 1X TBE at 25 $^{\circ}\text{C}$, 180 V, 35 min running time.

EMSA

Fluorescein attached native and Phe-ANH modified oligonucleotides were dissolved at a concentration of 10 nM in 10 μL of PBS buffer (pH 7.6) in the presence of 100 mM KCl. Samples were heated to 95 $^{\circ}\text{C}$ and cooled down to 5 $^{\circ}\text{C}$ at a rate of -1 $^{\circ}\text{C}/\text{min}$ before the thrombin additions. 2 equivalents of thrombin (from bovine plasma, sigma-aldrich) were added to the aptamer samples. After incubation for 1 hour at 5 $^{\circ}\text{C}$. After the incubation, 6Xloading dye (provided by NEB) was added to the protein-DNA complex solutions on ice. The analysis was conducted by electrophoresis in polyacrylamide gel. Electrophoresis was performed with a 8% polyacrylamide gel in 0.5XTBE

with 10 mM KCl buffer at 5 °C, 40 V, 4 hour running time.

SPR assays

SPR experiments were performed on a Biacore X instrument. A biotinylated ANHs-containing

TBA15 sequences were synthesized and a biotinylated native TBA15 was purchased from Sigma.

A streptavidin-functionalized SA sensor chip was purchased from Biacore. The biotinylated DNA is immobilized to the chip to obtain the desired immobilization level (approximately 100 RU rise).

SPR assays were carried out using HBS-EP buffer (10 mM HEPES-KOH pH 7.4, 150 mM NaCl,

3mM EDTA, and 0.005% Surfactant P20) with 100 mM KCl at 25°C. A series of sample solutions

with various concentrations were prepared in the buffer with 100 mM KCl and injected at a flow

rate of 20 ml/min. To measure the values of binding affinity and kinetics parameter, data processing

was performed with an appropriate fitting model using BIA evaluation 4.1 program. The predefined

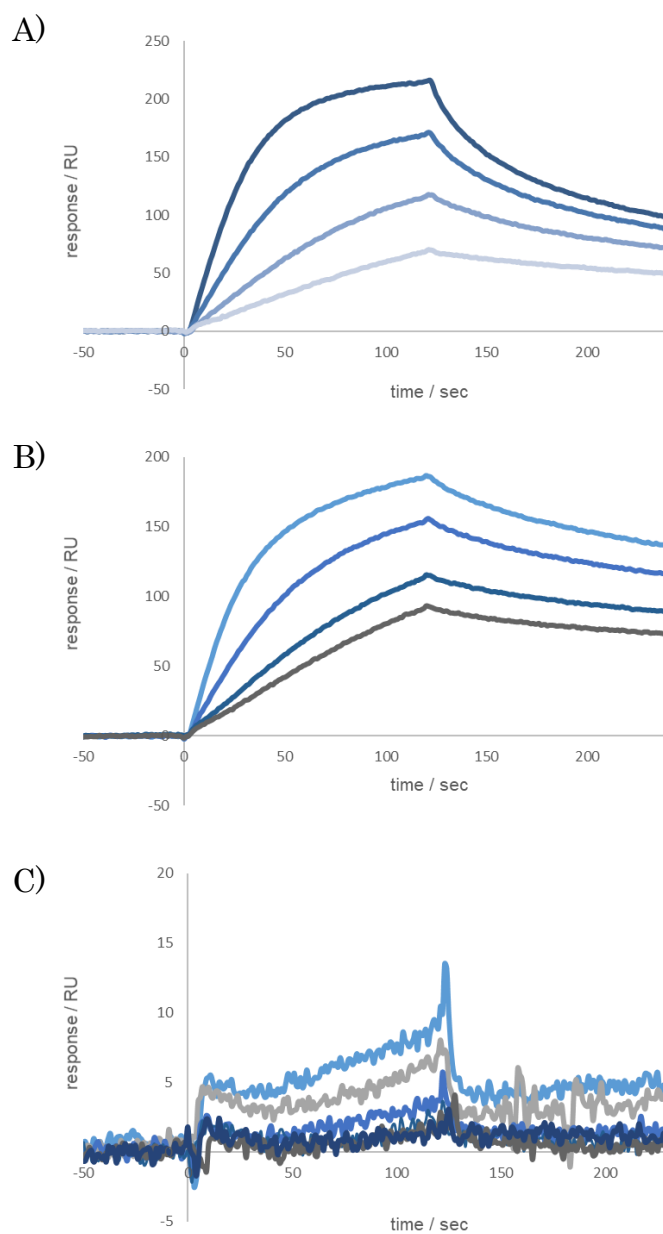
models (1:1 binding model with mass transfer or with drafting baseline) were used for fitting the

sensorgrams of TB to give better fitting. The sensorgram was fitted with the following model 1 to 1

equivalent.

Figure S9. SPR sensorgrams with the native and Phe-ANH containing TBA sequences ^a

^a Solution conditions: Various concentration of TB in HBS-EP buffer (10 mM HEPES-KOH pH 7.4, 150 mM NaCl, 3mM EDTA, and 0.005% Surfactant P20) with 100 mM KCl at 25°C.



A) SPR sensorgram of the native TBA sequence, B) SPR sensorgram of T3F TBA sequence, C) SPR sensorgram of T4F TBA sequence.

Molecular Modeling Study

Molecular modeling was carried out using the DS (Discovery Studio Client 2019) software package.

The site-specific ANH-modification TBA15 has conducted base on previously reported crystal structure (PDB ID: 1hao, 6EO6)^{S3}. We adopted 1hao as an initial structure for native TBA15

sequence simulation and 6EO6 as initial structure for Phe-modified TBA15. The building block of

Phe-ANH was prepared and minimized (RMS gradient: 0.001) 2 times to obtain the optimal

structure. The resulted Phe-ANH molecule was connected to the designated sequence of 6EO6.

Minimizations (3 independent runs) were operated for each models with CHARMM force field

parameters. The obtained structures were shown as Figure S10. Before MD calculations, harmonic

constrains were applied on G-quartet, then energy minimization was conducted. Subsequently, a

molecular simulation set, Standard Dynamic Cascade provided by DS software, was applied and

proceeded for the protein-DNA complexes. 'Standard Dynamic Cascade' undergoes following

procedure to operate the dynamic simulation. As the first step, two independent minimization

algorithms proceeded to obtain reliable initial structures; Adopted Basis NR as algorithm, 100000

max steps, RMS Gradient to be 0.001. Subsequent heating (from 50 K to 300 K) and equilibration

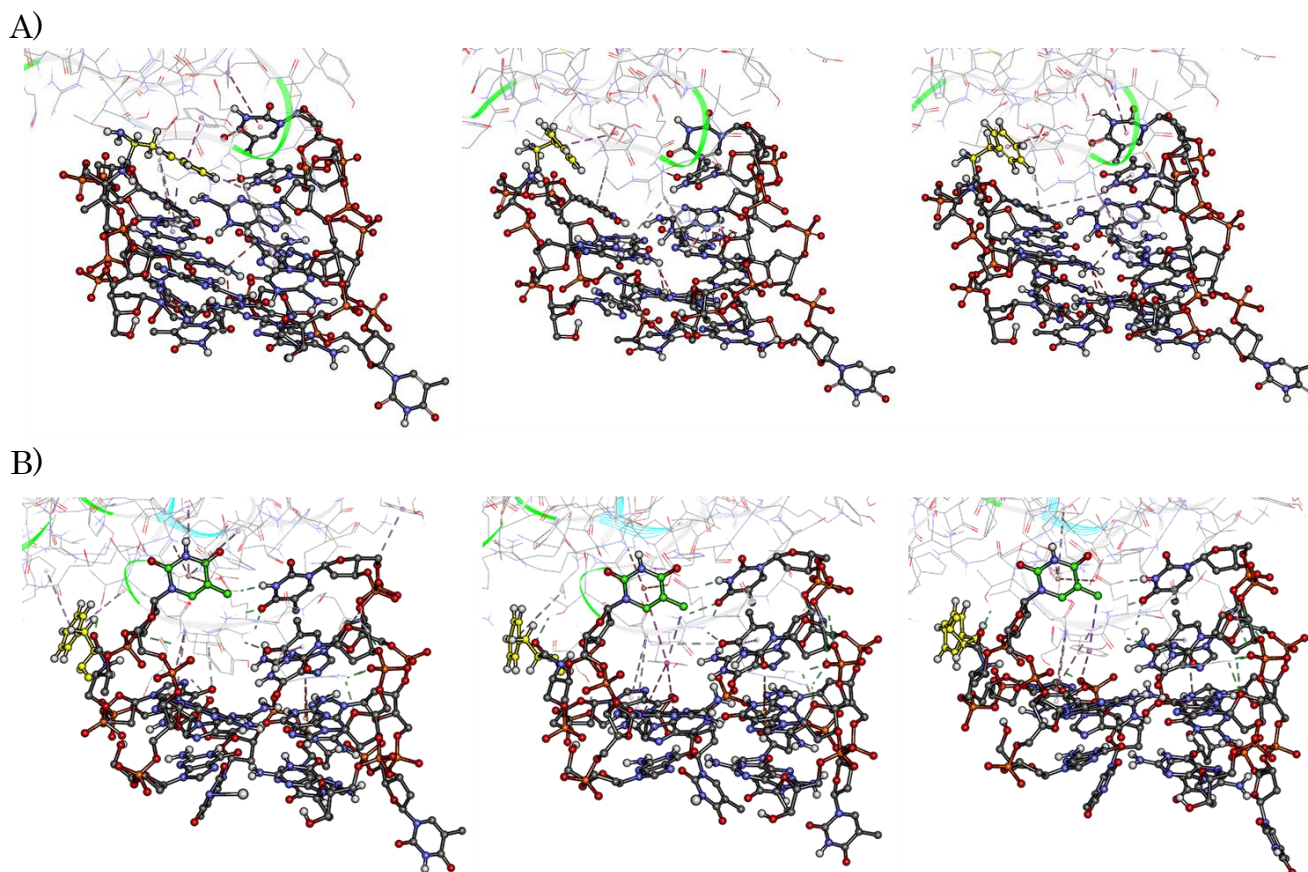
steps (0.1 fs as time steps during 100 ps simulation time, simulation temperature as 300 K) were

carried out. On the last stage, sampling was done with production step under certain conditions; 0.1

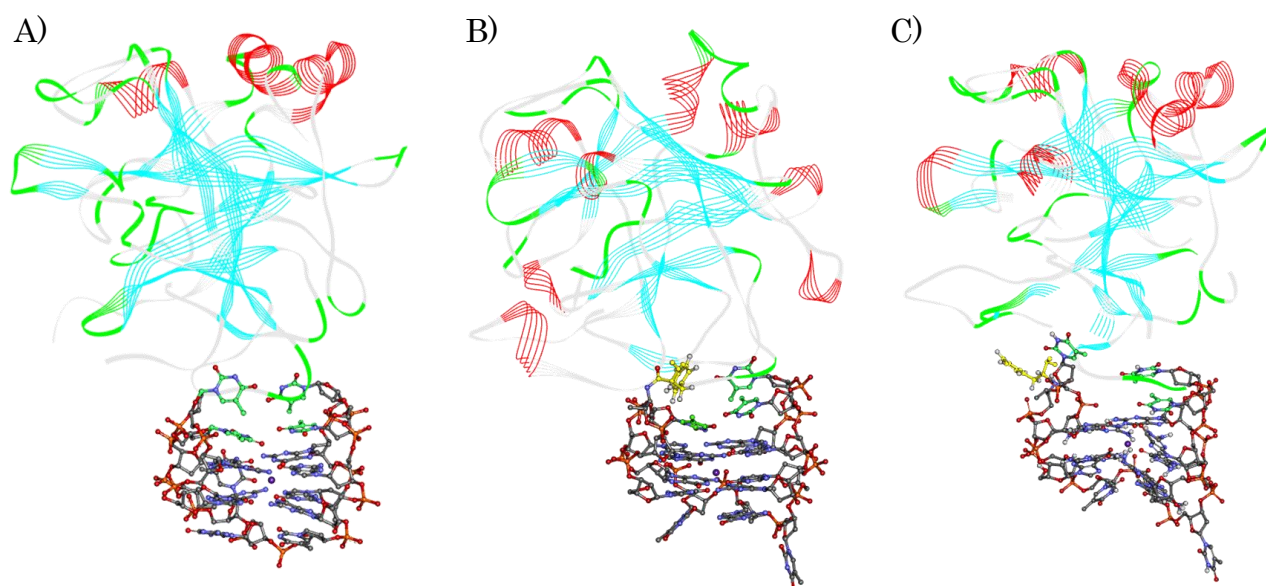
fs time steps during 10 ns and production temperature as 300 K. The resultants were displayed as

Figure S11.

Figure S10. The results of Phe-ANH containing TBA15 after several minimization



A) The energy minimized structure of T3F after multiple minimizations (1st, 2nd, and 3rd runs from left to right, PDB ID: 6EO6), B) The energy minimized structure of T4F after multiple minimizations (1st, 2nd, and 3rd runs from left to right, PDB ID: 6EO6).

Figure S11. Molecular dynamic results of the native, T3F, and T4F TBA with TB

A) Modeling results of the native TBA sequence with TB (PDB ID: 1hao), B) Modeling results of T3F TBA sequence with TB (PDB ID: 6EO6), C) Modeling results of T4F TBA sequence with TB (PDB ID: 6EO6).

References

- S1) K. Murayama, Y. Tanaka, T. Toda, H. Kashida, H. Asanuma, *Chem. Eur. J.* **2013**, *19*, 14151–14158.
- S2) S. Park, H. Matsui, K. Fukumoto, J. H. Yum, H. Sugiyama, *RSC Advances*, **2020**, *10*, 9717–9722.
- S3) R. Dolot, C. H. Lam, M. Sierant, Q. Zhao, F. W. Liu, B. Nawrot, M. Egli, X. Yang, *Nucleic Acids Res.* **2018**, *46*, 4819–4830.